Ocean Dynamics (2011) 61:873–880
DOI 10.1007/s10236-011-0386-7

Decadal variability of the Arctic Ocean thermal structure

Madhusoodanan M.S. · Bijoy Thompson

Received: 14 December 2009 / Accepted: 7 February 2011 / Published online: 6 April 2011

Abstract Long-term variability of heat content (HC) in the upper 1,000 m of the Arctic Ocean is investigated using surface and subsurface temperature and current data during 1958–2005 compiled by Simple Ocean Data Assimilation. Annual cycle of the Arctic Ocean HC is controlled primarily by the negative and positive excursions in net upper ocean heat flux, while the inter-annual variability is mainly associated with meridional thermal advection from the North Atlantic Ocean. Variability in HC is experienced as a basin-wide cooling/warming in association with the Arctic Oscillation on a decadal time scale. In the first three dominant modes of Empirical Orthogonal Function, the maximum amplitude of HC variability occurs in the Greenland–Norwegian Sea and Eurasian Basin. In general, HC showed increasing trend during 1958–2005 indicating continuous warming with regional variations in magnitude.

Keywords Arctic Ocean · Heat content · Ocean warming · Heat budget · EOF

1 Introduction

Climate changes and resulting variations of sea-ice thickness in the Arctic Ocean and exchange of heat and watermass between the Atlantic and Arctic Oceans are matters of serious global significance (Morison et al. 1998; Zhang et al. 1998; Johannessen et al. 1999; Comiso 2002; Hassol 2004). Sea-ice is an important component in the Arctic climate system as it controls the exchanges of heat, water, momentum, and gases across the ocean–atmosphere interface. Recent studies have shown that the Arctic ice sheet is thinning continuously (Rothrock et al. 1999; Walsh and Chapman 2001; Comiso 2002; Cavalieri et al. 2003; Kinnard et al. 2006, 2008). Sea-ice decline can lead to sea surface warming through increased absorption of solar radiation due to reduction in surface albedo. This promotes further ice melt and oceanic warming. Model studies by Lindsay and Zhang (2005) suggested that, rather than external forcing, the internal thermodynamical changes related to positive ice–albedo feedback dominate the Arctic sea ice thinning processes.

Studies have convincingly revealed that global upper ocean (1,000 m) temperature has increased by about 0.1°C during the period 1955–1995 due to increased emission of anthropogenic greenhouse gases to the earth's atmosphere (Levitus et al. 2000, 2001, 2005; Bindoff et al. 2007; Thompson et al. 2008). The Arctic Ocean has been warming during the past few decades (Polyakov et al. 2007; Zhang 2005, Steele et al. 2008). Quadfasel et al. (1991) reported anomalous warming of intermediate Atlantic water in the Nansen Basin in 1990. Using observational data sets, Polyakov et al. (2007) concluded that the Arctic Ocean is in transition to a warmer state and the reduction in Arctic ice cover may be an immediate implication of this warming. They suggested that the Arctic Ocean warming can have potential impacts on air–sea interaction processes occurring at low latitudes also. Zhang (2005) showed that the Arctic Ocean warms at a faster pace than the global average since 1960.

Responsible Editor: Pierre De Mey

M. M.S. (✉)
National University of Singapore, Physical Oceanography Research Laboratory, Tropical Marine Science Institute, Singapore, Singapore
e-mail: tmsmms@nus.edu.sg

B. Thompson
Department of Geological Sciences, Stockholm University, Stockholm, Sweden

The Arctic thermal variability is dominated by a decadal mode associated with the Arctic Oscillation (AO), which in turn is related to the North Atlantic Oscillation (NAO) and a low-frequency oscillation of about 60–80 years (Polyakov and Johnson 2000). The low-frequency variability in the North Atlantic is divided into four epochs, a negative epoch during 1870–1900, a positive epoch from 1900 to 1950 followed by another negative period from 1960 to 1980 and a second positive epoch from 1980 to present (Polyakov and Johnson 2000; Portis et al. 2001). The Arctic Ocean temperature showed significant changes during 1980s and 1990s. Eastern Arctic, Barents, and Greenland–Iceland–Norwegian Sea regions showed high sea surface temperatures in the 1950s, decreasing trend up to the 1960s and increase in subsequent decades (Polyakov and Johnson 2000). This pattern is in good agreement with the low-frequency variability in NAO. The Arctic Ocean temperature shows negative trend during the negative phase of AO/NAO (for instance, 1950–1980) and positive trend during the positive phase (for instance, from 1980 onwards).

This paper presents the long-term variability of heat content (HC) in the upper 1,000 m of the Arctic Ocean for the period 1958–2005. The area of study is the oceanic region north of 65° N. The heat budget and Empirical Orthogonal Function (EOF) analysis of HC anomalies are carried out to identify the dominant modes of variability. Upper ocean warming tendency of the Arctic Ocean is investigated on spatial and temporal scales.

2 Data used

Simple Ocean Data Assimilation (SODA) (Carton and Giese 2008) and gridded NCEP/NCAR reanalysis (Kalnay et al. 1996) data sets are used for the analysis. The SODA reanalysis consists of two experiments. The first one extends over a 44-year period from 1958–2001, using the ERA-40 data and the second one spans over the period of QuikSCAT scatterometry from 2000–November 2005. The reanalysis and associated experiments are available online in monthly averaged form, mapped into a uniform 0.5°×0.5°×40-level grid (http://ingrid.ldeo.columbia.edu/SOURCES/.CARTON-GIESE/.SODA/.v2p0p2-3). The surface and subsurface temperatures, and the meridional and vertical velocity data from SODA are used in this study. The assimilation procedures and data evaluation have been detailed in Carton and Giese (2008). The NCEP/NCAR reanalysis variables consist of three types, those are well constrained by observations, those partly constrained by dynamical relationships to variables that are frequently observed, and those variables such as horizontal velocity divergence that are poorly constrained and may contain significant errors. The variables such as wind, temperature, and geopotential height are strongly influenced by the assimilated observations and they accurately represent the Arctic atmosphere (Overland et al. 1997). Serreze et al. (1998) and Walsh and Chapman (1998) confirmed that NCEP/NCAR reanalysis correctly represent the spatial patterns and seasonal variations though the magnitudes were higher than observed values.

3 Results

3.1 Heat budget of the Arctic Ocean

Due to its geographical location around the North Pole, Arctic Ocean is almost surrounded by land-mass except at the opening to Atlantic Ocean (through Fram Strait) and Pacific Ocean (through Bering Strait). Salt and heat exchanges between the Arctic and Atlantic oceans take place mainly through the Greenland–Iceland–Norwegian Sea. Using horizontal and vertical velocity and temperature data from SODA, heat budget of the upper 1,000 m of the Arctic Ocean has been estimated. Exchange of heat between the control volume and surrounding occurs through the southern boundary at 65° N, across the air–sea interface and through the bottom at 1,000 m. The oceanic heat balance is given as

$$dQt = Q^{\mathrm{adv}} + Q^{\mathrm{diff}} + Q^{\mathrm{flx}} \tag{1}$$

where dQt is the rate of change of oceanic (1,000 m) heat content (heat content tendency), Q^{adv} is the sum of flux contribution across 65° N and 1,000 m depth of control volume, Q^{diff} is the diffusive heat at bottom of control volume, and Q^{flx} is the net surface heat flux. The heat content is computed as

$$Q = \int_{z=0}^{z=1{,}000} \rho\, C_{\mathrm{p}}\, T_{\mathrm{z}}\, dz \tag{2}$$

here ρ_{w}=1,026 kg m^{-3} is the density of seawater, C_{p}= 3,902 J kg^{-1} K^{-1} is the specific heat capacity of the sea water, and T_{z} is the ocean temperature.

Net downward shortwave radiation, net upward longwave radiation, sensible heat flux, and latent heat flux are taken from NCEP/NCAR reanalysis for computing the net surface heat flux. Positive net heat flux is the heat transferring into the ocean. The SODA data is used for the computation of dQt, Q^{adv} and Q^{diff}. Fluxes Q^{adv} and Q^{diff} are computed based on the formulations by Shenoi et al. (2005). The advective flux can be estimated as the sum

of flux across the southern boundary of the control volume (65° N) due to meridional velocity (v) and flux across the bottom of the control volume due to vertical velocity (w).

$$Q^{\mathrm{adv}} = -\frac{\rho_{\mathrm{w}} C_{\mathrm{p}}}{A}\left[\int_x\int_z T_{65}\, v_{65}\, dz\, dx + \int_x\int_y T_{1{,}000} w_{1{,}000}\, dy\, dx\right] \tag{3}$$

The diffusive flux through bottom of the control volume is calculated as

$$Q^{\mathrm{diff}} = -\frac{\rho_{\mathrm{w}} C_{\mathrm{p}}\, k}{A}\left[\int_x\int_y \frac{dT}{dz}\, dx\, dy\right] \tag{4}$$

where T_{65} and v_{65} are temperature and meridional velocity at 65° N, $T_{1,000}$ and $w_{1,000}$ are temperature and vertical velocity at 1,000 m, k=2×10^{-4} m^2 s^{-1}, A is area of the control volume at the ocean surface, and $\frac{dT}{dz}$ is computed at 1,000 m depth.

The principal objective of this exercise is to understand the long-term variability of the Arctic Ocean heat content. We are aware of the fact that critical use of ocean reanalysis data may lead to re-evaluation of contribution of various terms in heat budget. Due to this limitation, we try to approach the budget in its qualitative aspect rather than a quantitative one. SODA reanalysis data has been used successfully for the heat budget analysis of the Arabian Sea and the Bay of Bengal (Shenoi et al. 2005) and the equatorial Indian Ocean (Chowdary and Gnanaseelan 2007). Before doing more analysis, it will be relevant to check the heat balance of the data. We look into the climatology and inter-annual variability of the heat budget components. The climatology of heat budget components of the Arctic Ocean is presented in Fig. 1. Annual cycle of the Arctic Ocean heat content tendency is characterized by a single maximum and minimum. Heat content tendency has positive values during April–September. It gradually increases from winter to a maximum in July and decreases thereafter. The major component in the Arctic Ocean heat budget is the horizontal advection from the Atlantic and Pacific oceans. Contribution from heat transport through the Bering Strait is relatively small. Seasonal variation in vertical advection (through the bottom surface) is very small, where heat flux of about 5 W m^{-2} is lost from the control volume throughout the year. The contribution from temperature diffusion at bottom of the volume is negligibly small compared to other components. Further, the lateral diffusive fluxes across the southern boundary are almost negligible (of the order of 10^{-6}). Hence, the contributions from lateral diffusive fluxes are not taken into account in the budget analysis. The meridional advection consistently maintains value above 45 W m^{-2} irrespective of the seasons.

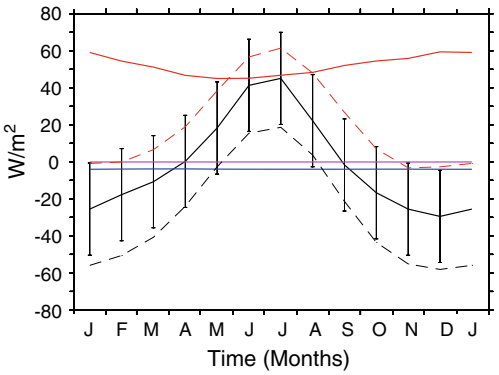

Fig. 1 The climatological heat budget of the Arctic Ocean for the upper 1,000 m. The individual heat budget components shown are heat content tendency (*black line*), meridional advection (*red line*), vertical diffusion at 1,000 m (*purple line*), vertical advection at 1,000 m (*blue line*), and NCEP/NCAR net surface heat flux (*black dashed line*). The SODA data is used for the computation of heat content tendency, meridional and vertical advections, and vertical diffusion. The sum of advection, diffusion, and net surface heat flux is shown as *red dashed line*. The standard deviation of heat content tendency is drawn as *vertical lines*

The meridional advection is highest during the winter (December–February). This is consistent with the observational study by Schauer et al. (2004). The striking feature is that the meridional advection shows minimum contribution during June, whereas the heat content tendency reaches its maximum in July. The maximum insolation over Arctic region occurs during June–July (Serreze et al. 1998). The net surface heat flux computed from NCEP/NCAR reanalysis data also reaches its maximum almost during the same time. This shows that increase in the Arctic Ocean heat content tendency is driven by the change in net heat flux. The surface net heat flux is the key factor that brings strong seasonal variability in oceanic heat content tendency. Also, it should be noted that the seasonal variability in the meridional heat advection is out of phase with the HC variability.

In this analysis, however, the budget is not closed and has a maximum imbalance of about 30 W m^{-2} during November–December. Since the assimilation of data acts as a source of temperature and salinity at surface and subsurface, heat fluxes calculated with bulk formulae yield a misleading impression on the temperature changes. This can possibly be overcome by calculating heat and freshwater fluxes diagnostically using the sum of storage, divergence of transport, and diffusion (James Carton, personal communication). In spite of the imbalance in budget, the encouraging fact in the present study is that net heat flux and heat content tendency follows identical patterns of variability.

The seasonal cycles were removed from the heat budget components before doing the analysis of their inter-annual variability. The anomalies of heat content tendency,

meridional advection, and net surface heat flux over the Arctic Ocean for the study period are shown in Fig. 2. The high-frequency signals were removed from the heat budget components by applying a 2-year running filter. The figure shows that the meridional advection and the net heat flux anomalies are varying almost in phase with the heat tendency anomaly. However, in a few occasions they act in opposite phases. For instance, during 1972–1973 and 2003 the meridional advection and net heat flux shows positive anomalies, while the heat content tendency anomaly tends to be negative.

It is seen that significant correlations of 0.52 and 0.33 exists between the filtered anomalies of meridional advection and heat content tendency, and between the filtered anomalies of net surface heat flux and heat content tendency, respectively, which are above 1% significance level. Different from climatological heat budget, the correlation analysis reveals that in inter-annual time scale the meridional advection play a dominant role in the Arctic Ocean HC variability. Earlier, the analysis of mooring observations by Schauer et al. (2004) showed significant inter-annual variability in annual mean heat transport across the Fram strait. Interestingly, the correlation between the anomalies of heat content tendency, and the sum of meridional advection and net surface heat flux has not shown a remarkable increase (correlation=0.53). This result also emphasizes the dominant effect of meridional advection on the Arctic Ocean heat content variability in inter-annual time scales.

3.2 Arctic Ocean heat content variability

The annual average of climatological 1,000 m HC in the Arctic Ocean is shown in Fig. 3a. HC climatology shows very small spatial variability at seasonal timescale (not shown). Due to the transport of warm Atlantic water HC

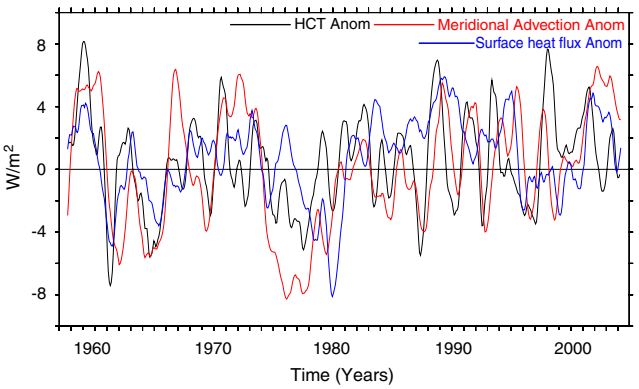

Fig. 2 The inter-annual variability in the heat budget components (in watts per square meter) of the Arctic Ocean for the upper 1,000 m. The anomalies of heat content tendency (*HCT Anom*, *black line*) and meridional advection (*red line*) are computed using SODA and net surface heat flux anomaly (*blue line*) is computed from NCEP/NCAR reanalysis

maximum is seen in the Eurasian Basin, particularly over the Greenland–Norwegian Sea region, Nansen Basin, and Amundsen Basin regions. While analyzing the 1,000 m HC, it should be noted that large area of the Arctic Ocean has depth below 500 m, where HC is also remarkably small. Larger ocean depth variations can lead to misinterpretation of results. In this context, long-term variability of the Arctic Ocean HC can be studied more clearly using the anomalies. EOF analysis is used to identify dominant modes of variability present in heat content anomaly (HCA). The first dominant mode of variability in HCA is characterized by uniform polarity over most of the Arctic Ocean, which explains 19% of the total variability (Fig. 3b). This mode is associated with basin-wide cooling or warming in the Arctic Ocean. The maximum amplitude of variability is found to be located over the Iceland Sea, Fram Strait, and Nansen Basin. The second and third dominant modes of HCA variability are shown in Fig. 3c and d. These two modes explain 9% and 8% of the total variability, respectively. The second mode has a strong positive loading in the Norwegian and Eurasian basins. This mode corresponds to warming/cooling in the Norwegian and Eurasian basins and weak cooling/warming in other regions, whereas the third dominant mode shows equally strong positive and negative loadings over the entire Arctic Ocean. Peak amplitude of this variability is seen in the Norwegian Basin. Figure 3b, c, and d show that in the first three dominant modes of HCA, significant variability is seen in the Greenland–Norwegian basins and adjacent Eurasian Basin. These are regions where exchange of watermass takes place between the Atlantic and Arctic Oceans.

The EOF time amplitude functions (TAF) of first (black line), second (red line), and third (blue line) dominant modes of variability in HCA are shown in Fig. 4. The dominant modes of variability in the Arctic Ocean HCA show oscillations of about 3–10 years. FFT analysis was carried out to isolate the different modes of oscillations in the time series. TAF of EOF1 (Fig. 5) exhibits a low-frequency oscillation of decadal time scale. The FFT power spectrum shows strong low-frequency oscillation of about 114 months. Over the entire Arctic basin, positive values of TAF are characterized by positive anomaly in HCA and vice versa. Oscillations of timescales 36 and 58 months are also prominent in the EOF1 of HCA. FFT power spectra of EOF2 (Fig. 5) is marked by the presence of oscillations of 28, 38, and 59 months, while EOF3 time amplitude functions show oscillations of 24, 36, and 44 months. Temporal occurrence of HC variability shifts towards higher frequency side in the less dominant EOF modes. The TAF of EOF1 follows EOF2 with time lag of 1–2 years (Fig. 4). This implies that the changes in the Arctic Ocean heat content in inter-annual timescales are appearing in the

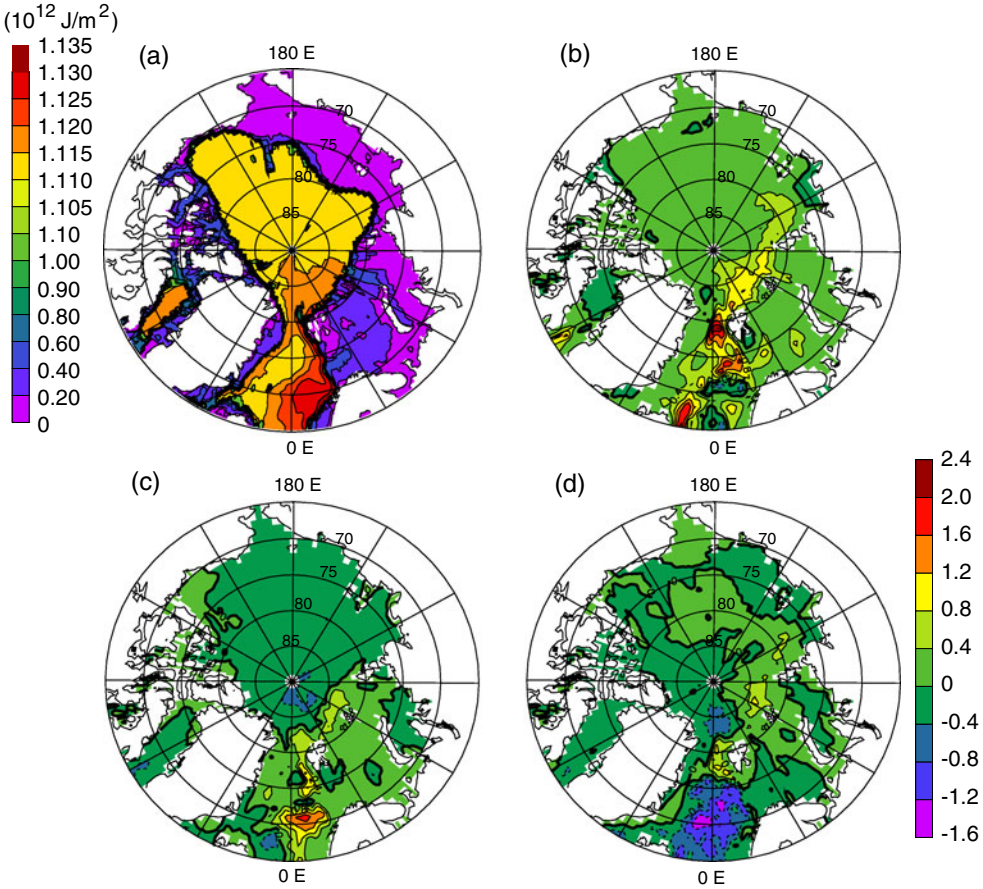

Fig. 3 The heat content and EOF of heat content anomalies for the Arctic Ocean. **a** The annual climatology of the upper 1,000 m heat content for the Arctic Ocean (10^{12} J m^{-2}). The first (**b**), second (**c**), and third (**d**) dominant modes of heat content variability for the Arctic Ocean. The shading legend corresponds to (**a**) is shown in its *left side*. The *color bar* shown at the right side of (**d**) is common to (**b**), (**c**), and (**d**)

form of propagating anomalies from the Atlantic Ocean. The water from the Atlantic Ocean flows into the Barents Sea and to the Canadian Basin through the Eurasian Basin. Polyakov et al. (2007) observed that the temperature anomaly took about 1.5 years to propagate from the Norwegian Sea to Fram Strait region and about 4.5–5 years to reach the Leptev Sea. The presence of relatively high frequency oscillations in the TAF of EOF2 in the FFT analysis further confirms this result. These results emphasize that the meridional heat transport from the Atlantic Ocean has important implications on the low-frequency variability in the Arctic Ocean heat content.

3.3 Increasing trend in the Arctic Ocean heat content

The Arctic Ocean 1,000 m HC shows an increasing trend during the period from 1958 to 2005 with conspicuous spatial variations. Sharp increase is seen over the Icelandic Sea and Fram Strait regions (Fig. 6a). Slightly negative trend is encountered only in the Norwegian Sea. The 1,000 m HC for unit area of the Arctic Ocean is plotted in the Fig. 7. The

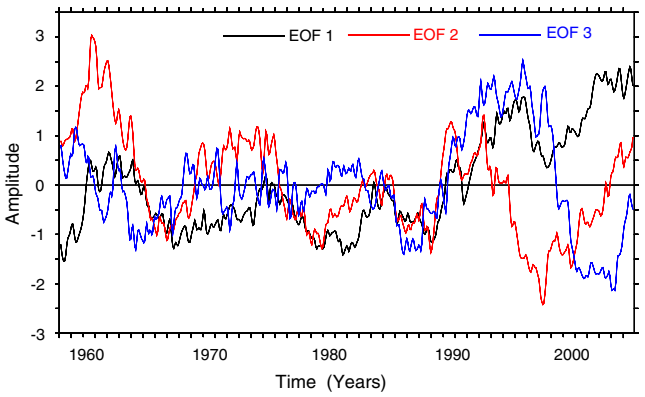

Fig. 4 The time amplitude functions for EOF1 (*black line*), EOF2 (*red line*), and EOF3 (*blue line*) of the Arctic Ocean 1,000 m heat content anomalies

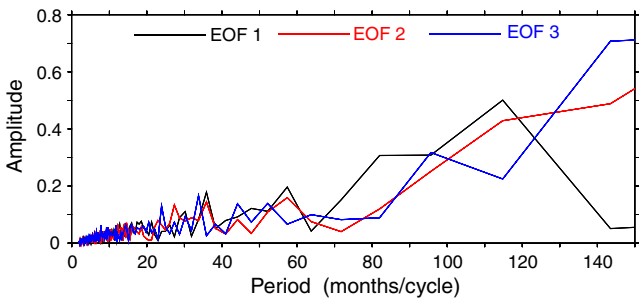

Fig. 5 The FFT power spectrum of time amplitude function for EOF1 (*black line*), EOF2 (*red line*) and EOF3 (*blue line*) of the Arctic Ocean 1,000 m heat content anomalies

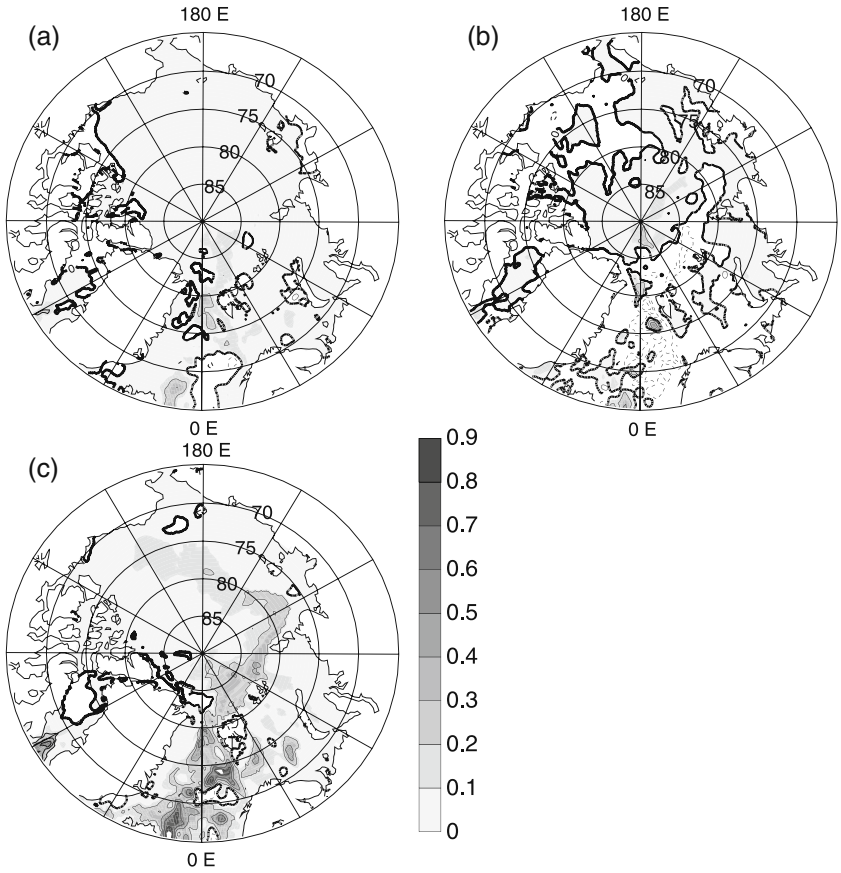

Fig. 6 The linear trends in the upper 1,000 m heat content (10^6 J m^{-2} per year) **a** during 1958–2005, **b** 1958–1979, and **c** 1980–2005. Only positive values are *shaded*

linear trend-line is also shown. The linear increase is of the order of 7.93×10^6 J m^{-2} per year. HC exhibits two distinct epochs on either side of 1980 with a gradual decrease till 1980 and a sharp increase thereafter. The spatial distribution also shows significant variations during pre- and post-1980s (Fig. 6b and c). In the Norwegian Sea and central Eurasian Basin the trends are almost opposite. During pre-1980s, even though the spatial extend of HC increasing and decreasing trend are almost equal, the strong decreasing trend in the central Eurasian Basin dominates over the weak increasing trend. Post-1980 increase in HC is sharp in the Iceland–Norwegian Sea, Fram Strait, Barent Sea, and central Eurasian Basin. The HC shows a linear increasing trend of 7.4×10^8 J m^{-2} in post-1980s, while the trend was -2×10^8 J m^{-2} during pre-1980s.

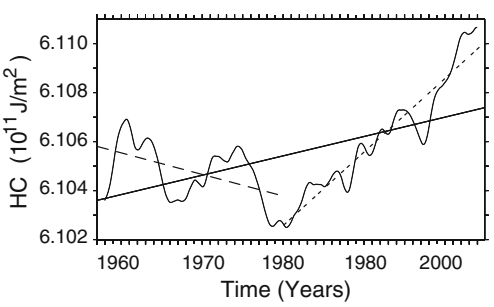

Fig. 7 The upper 1,000 m heat content per unit area for the Arctic Ocean. The linear trends during the period 1958–2005 (*black continuous line*), 1958–1979 (*black dashed line*), and 1980–2005 (*black dotted line*) are also drawn in the figure. The time series is low-pass filtered with a 2-year running filter

4 Discussions and conclusion

Global warming and consequent decrease in the Arctic sea-ice cover are major concerns to climate researchers as well as policy makers. Complex bathymetry, geographical position around the pole, abundant inflow of freshwater from the Canadian and Siberian rivers, and limited connections to other world oceans are crucial factors that determine the thermodynamics of the Arctic Ocean. Our knowledge on subsurface temperature and circulation in the Arctic Ocean is very limited due to scarcity of data.

In the present study, we tried to estimate the Arctic Ocean upper level heat content, its long-term variability and influence of watermass advection from the North Atlantic Ocean. Temperature and current data from Simple Ocean Data Assimilation reanalysis datasets were used. The annual cycle of heat content tendency shows a positive maximum during boreal summer (June–August) and a negative minimum

during boreal winter (December–February). The meridional advection of heat from the North Atlantic Ocean has a major influence on the Arctic Ocean heat budget climatology. The contribution from vertical diffusion at bottom (1,000 m) of the control volume is negligibly small compared to other terms. The seasonal variability in meridional advection is relatively small compared to net surface heat flux and heat content tendency. The anomalies of meridional heat advection from the North Atlantic Ocean are significantly correlated to the Arctic Ocean heat content.

The first dominant mode of heat content variability over the Arctic Ocean is characterized by basin-wide cooling or warming, which explains 19% of the total variability. The second and third dominant modes explain 9% and 8% of the total variability, respectively. The first three dominant modes of heat content anomaly show maximum amplitude of variability in the Greenland–Norwegian Sea and Eurasian Basin, emphasizing that the Arctic Ocean variability is strongly influenced by the North Atlantic Ocean. The first dominant mode of heat content variability shows oscillation with frequency around 10 years. This decadal mode of oscillation is associated with the Arctic Oscillation (Polyakov and Johnson 2000). The oscillations shift towards higher frequency side in the second and third dominant modes of HC variability.

The Arctic Ocean heat content shows a linear increasing trend of 7.93×10^6 J m^{-2} per year. Interestingly, the heat content gradually decreases pre-1980s and increases rapidly thereafter. The increasing trend is sharper after mid-1990s. The spatial distribution of linear trend in heat content exhibits opposite trends during pre- and post-1980.

Acknowledgments The research work of Bijoy Thompson is supported by Bert Bolin Center for Climate Research (BBCC), Stockholm University, Sweden. Madhusoodanan thanks NUS and NERCI for support. Datasets are obtained from http://ingrid.ldeo.columbia.edu data library. We acknowledge the two anonymous reviewers for their invaluable comments, which improved the original manuscript. The figures are drawn using Ferret.

References

Bindoff NL, et al. (2007) "Observations: Oceanic Climate Change and Sea Level." In: Climate Change 2007: The Physical Science Basis. Contribution of Working Group I to the Fourth Assessment Report of the Intergovernmental Panel on Climate Change [Solomon S, Qin D, Manning M, Chen Z, Marquis M, Averyt KB, Tignor M, Miller HL (eds.)] (Cambridge, United Kingdom and New York, NY, USA: Cambridge University Press)

Carton JA, Giese BS (2008) A reanalysis of ocean climate using Simple Ocean Data Assimilation (SODA). Mon Wea Rev 136:2999–3017

Cavalieri DJ, Parkinson CL, Vinnikov KY (2003) 30-Year satellite record reveals contrasting Arctic and Antarctic decadal sea ice variability. Geophys Res Lett. doi:10.1029/2003GL018031

Chowdary JS, Gnanaseelan C (2007) Basin-wide warming of the Indian Ocean during El Niño and Indian Ocean Dipole years. Int J Clim 27(11):1421–1438

Comiso JC (2002) A rapidly declining perennial sea ice cover in the Arctic. Geophys Res Lett. doi:10.1029/2002GL015650

Hassol SJ (2004) *Impacts of a Warming Arctic: Arctic Climate Impact Assessment*. Cambridge University Press, Cambridge.

Johannessen OM, Shalina EV, Miles MW (1999) Satellite Evidence for an Arctic Sea Ice Cover in Transformation. Science. doi:10.1126/science.286.5446.1937

Kalnay E et al. (1996) The NCEP/NCAR 40-year reanalysis project. Bull Am Meteorol Soc. 77:437–471

Kinnard C, Zdanowicz CM, Fisher DA, Wake CP (2006) Calibration of an ice-core glaciochemical (sea-salt) record with sea-ice variability in the Canadian Arctic. Annals of Glaciology 44:383–390

Kinnard C, Zdanowicz CM, Koerner R, Fisher DA, (2008) A changing Arctic seasonal ice zone -Observations from 1870–2003 and possible oceanographic consequences. Geophys Res Lett. doi:10.1029/2007GL032507

Levitus S, Antonov J, Boyer TP (2000) Warming of the world ocean. Science 287:2225–2229

Levitus S, Antonov JL, Wang J, Delworth TL, Dixon KW, Broccoli AJ (2001) Anthropogenic warming of Earth's climate system. Science 292:267–270

Levitus S, Antonov J, Boyer TP (2005) Warming of the world ocean, 1955–2003. Geophys Res Lett. 32. doi:10.1029/2004GL021592

Lindsay RW, Zhang J (2005) The thinning of arctic sea ice, 1988–2003: have we passed a tipping point? J Clim 18:4879–4894

Morison J, Steele M, Anderson R (1998) Hydrography of the upper Arctic Ocean measured from the nuclear submarine USS Pargo. Deep-Sea Res 45:15–38

Overland JE, Adams JM, Bond NA (1997) Regional variation of winter temperatures in the Arctic. J Clim 10(5):821–837

Polyakov IV, and Johnson MA (2000) Arctic decadal and inter-decadal variability. Geophys Res Lett 27:4097–4100

Polyakov IV et al. (2007) Observational Program Tracks Arctic Ocean Transition to a Warmer State. Eos Trans. AGU. doi:10.1029/2007EO400002

Portis DH, Walsh JE, El Hamly M, Lamb PJ (2001) Seasonality of the North Atlantic Oscillation. J Clim 14:2069–2078

Quadfasel D, Sy A, Wells D, Tunik A (1991) *Warming in the Arctic.* Nature. 350:385

Rothrock DA, Yu Y, Maykut GA (1999) Thinning of the Arctic Sea-Ice Cover. Geophys Res Lett 26(23):3469–3472

Schauer U, Fahrbach E, Osterhus S, Rohardt G (2004) Arctic warming through the Fram Strait: oceanic heat transport from 3 years of measurements, J. Geophys. Res., 109, C06026, doi:10.1029/2003JC001823

Serreze MC, Key J, Box J, Maslanik J, Steffen K (1998) A new monthly climatology of global radiation for the Arctic and comparisons with NCEP-NCAR reanalysis and ISCCP-C2 fields. J Clim 11(2):121–136

Shenoi SSC, Shankar D, Shetye SR (2005) On the Accuracy of the simple ocean data assimilation analysis for estimating heat budgets of the near-surface Arabian Sea and Bay of Bengal, J. Phys. Oceanogr 35(3):395–400

Steele M, Ermold W, Zhang J (2008) Arctic Ocean surface warming trends over the past 100 years. Geophys Res Lett. doi:10.1029/2007GL031651

Thompson B, Gnanaseelan C, Parekh A, Salvekar PS (2008) North Indian Ocean warming and sea level rise in an OGCM. J Ear Sys Sci 117:169–178

Walsh JE, Chapman WL (1998) Arctic cloud-radiation-temperature associations in observational data and atmospheric reanalyses. J Clim 11:3030–3045

Walsh JE, Chapman WL (2001) Twentieth-century sea ice variations from observational data. Ann Glaciology 33:444–448.

Zhang J (2005) Warming of the arctic ice-ocean system is faster than the global average since the 1960s. Geophys Res Lett. doi:10.1029/2005GL024216

Zhang J, Rothrock DA, Steele M (1998) Warming of the Arctic Ocean by a strengthened Atlantic inflow: Model results. Geophys Res Lett 25:1745–1748